Int. J. Heat Mass Transfer. Vol. 36, No. 9, pp. 2271–2279, 1993
Printed in Great Britain

0017-9310/93 $6.00+0.00

A unified model for the prediction of bubble detachment diameters in boiling systems—II. Flow boiling

L. Z. ZENG, J. F. KLAUSNER, D. M. BERNHARD and R. MEI†
University of Florida, Department of Mechanical Engineering, Gainesville, FL 32611, U.S.A.

(*Received* 5 *August* 1992 *and in final form* 12 *November* 1992)

Abstract—An improved model is proposed for the prediction of departure and lift-off diameters in saturated forced convection boiling. The model utilizes a force balance similar to that proposed by Klausner *et al.* (*Int. J. Heat Mass Transfer* **36**, 651–662 (1993)). One significant improvement is that the inclination angle is determined on a dynamic basis and is not required as an input. Furthermore, it is hypothesized that the surface tension force is small compared to other forces acting on a vapor bubble at the points of departure and lift-off, and thus information on the bubble contact diameter and contact angles is not required. A new data set on mean vapor bubble lift-off diameters and probability density functions (pdf's) for flow boiling of refrigerant R113 on a nichrome heating strip has been obtained using the experimental facility described by Klausner *et al.* (*Int. J. Heat Mass Transfer* **36**, 651–662 (1993)). The wall superheat and mean liquid velocity respectively range from 5.5 to 12.0°C and 0.35 to 1.0 m s^{-1}. It is demonstrated that over the limited range of flow boiling conditions considered, the predicted departure and lift-off diameters agree well with measured values.

1. INTRODUCTION

DUE TO the difficulties in experimental measurements and analytical modelling, the study of vapor bubble detachment in forced convection boiling has received little attention in the literature when compared with pool boiling despite its importance in understanding the microconvection component of heat transfer. A survey of those investigators [1–3] who have considered vapor bubble detachment in flow boiling is given by Klausner *et al.* [4]. As was mentioned in refs. [4] and [5], vapor bubbles in flow boiling systems typically detach from their nucleation sites via sliding, and lift off the heating surface downstream from the nucleation site. The instant at which a vapor bubble detaches from its nucleation site is referred to as the point of departure and the instant it detaches from the heating surface is referred to as the lift-off point. The forces acting on a growing vapor bubble in boiling systems were discussed in detail in ref. [4]. Since the vapor bubble detachment correlations found in refs. [1–3] do not discriminate between the point of departure and lift-off, they will not be considered here.

In ref. [4] it was demonstrated that while a vapor bubble is attached to its nucleation site it grows asymmetrically. The asymmetrical growth was modelled by considering a vapor bubble growing at an inclined angle θ_i as depicted schematically in Fig. 1. θ_i is referred to as the inclination angle. In order to evaluate the force due to bubble growth acting in the direction of flow (x-direction) or normal to the heating surface (y-direction), knowledge of the inclination angle is required. One significant improvement of the present model over that presented in ref. [4] is that θ_i is determined as part of the solution, as opposed to treating it as an empirical constant.

Expressions were given in ref. [4] for evaluating the surface tension forces acting in the x- and y-directions on a vapor bubble in flow boiling. As the contact diameter, d_w, approaches zero, the surface tension forces are negligible. When considering pool boiling vapor bubble departure in ref. [5], it was hypothesized that near the point of departure the contact diameter is sufficiently small such that the surface tension force is negligible compared with the growth and buoyancy forces. The same hypothesis is made here to flow boiling, but definitive proof is lacking. The present vapor bubble departure and lift-off model neglects the surface tension compared with other forces, and thus the usefulness of the model must be judged based on its agreement with the limited available experimental

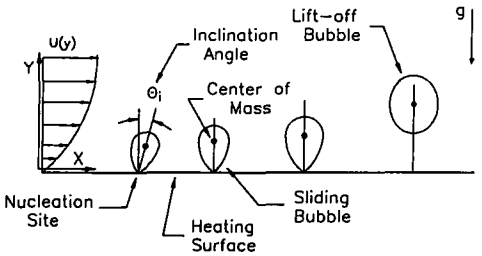

FIG. 1. Schematic diagram of vapor bubble departure and lift-off.

† Department of Aerospace Engineering, Mechanics and Engineering Science.

NOMENCLATURE

a vapor bubble radius [m or mm]
C_p specific heat [J kg^{-1} C^{-1}]
d_d vapor bubble departure diameter [m or mm]
d_L vapor bubble lift-off diameter [m or mm]
d_w surface/bubble contact diameter [m]
D inside dimension of square channel [m]
G mass flux [kg m^{-2} s^{-1}]
h_{fg} latent heat of vaporization [J kg^{-1}]
q_w wall heat flux [kW m^{-2}]
r_r radius of curvature of bubble at its base [m]
T_{sat} saturation temperature [°C]
ΔT_{sat} wall superheat [°C]
t time [s or ms]
u area averaged velocity [m s^{-1}]
$U(y)$ liquid velocity profile near wall [m s^{-1}]
ΔU velocity difference between bubble center of mass and surrounding liquid [m s^{-1}]
u^* friction velocity [m s^{-1}]
X vapor quality.

Greek symbols
δ liquid film thickness [m or mm]
θ_i inclination angle
ν liquid kinematic viscosity [m^2 s^{-1}]
ρ density [kg m^{-3}]
σ surface tension [N m^{-1}].

Subscripts
l liquid
v vapor.

data. The use of this hypothesis greatly simplifies the prediction of departure and lift-off diameters since knowledge of the contact diameter and advancing and receding contact angles are not required.

Although an analytical vapor bubble departure and lift-off model was formulated in ref. [4], it was only tested against departure data; lift-off data were not available. Since then, vapor bubble lift-off data have been obtained for flow boiling of R113 in a pyrex 25 × 25 mm square channel. The experimental facility which was described in detail in ref. [4] was used to collect the data. The length of the longest chord parallel to the heating surface which bisects the vapor bubble is taken to be the characteristic bubble diameter. 'Probability density functions' (pdf's) for vapor bubble lift-off have been obtained for wall superheat, ΔT_{sat}, ranging from 5.5 to 12.0°C and mean liquid velocity, u_l, ranging from 0.35 to 1.0 m s^{-1}. The upper limit on wall superheat was constrained by the ability to visually distinguish vapor bubble lift-off.

Probability density functions obtained for vapor bubble *lift-off* indicate that the lift-off process is strongly dependent on wall superheat and weakly dependent on liquid velocity. This observation is in strong contrast to the vapor bubble *departure* process described in ref. [4] in which vapor bubble departure diameters are strongly dependent on both wall superheat and liquid velocity. In this work, the analytical model developed in ref. [4] is modified to predict both vapor bubble departure and lift-off diameters in flow boiling systems. A comparison between the measured and predicted departure and lift-off diameters shows good agreement for horizontal flow boiling.

2. VAPOR BUBBLE LIFT-OFF DATA

The experimental facility used to collect vapor bubble lift-off diameters and methodology for data collection were described in detail in ref. [4] and are not repeated here. The diameter of the bubble which just detaches from the heating surface is taken to be the lift-off diameter. The uncertainty in the lift-off diameter measurement is ±0.03 mm. In order to construct a pdf, at least 200 independent measurements of vapor bubble lift-off diameters are acquired. For all of the measurements obtained, the two-phase flow regime was stratified and the boiling regime was that of isolated bubbles. Probability density functions, expressed in terms of the number of bubbles at a given diameter normalized by the total number, are shown in Figs. 2(a) and (b) for vapor bubble lift-off diameters at constant wall superheat and various liquid velocities. In Fig. 2(a) the mean wall superheat, ΔT_{sat}, is maintained at 8°C while that in Fig. 2(b) is maintained at 10°C. In Fig. 2(a) the pdf's are slightly scattered. However, it is important to note that there is no apparent dependence of the lift-off diameters on the liquid velocity. In Fig. 2(b), it is more evident that the mean lift-off diameter is independent of the liquid velocity. One interesting feature displayed by these lift-off pdf's is that the standard deviation from the mean is typically about half the standard deviation for the corresponding departure pdf's presented in ref. [4]. It was postulated in ref. [4] that the observed distribution of departure diameters was due to the apparently random instantaneous liquid velocity and local wall superheat seen by a growing vapor bubble. Should the instantaneous velocity exert only a weak influence on the lift-off process, it is expected that the standard deviation for lift-off be less than that for departure, as has been observed. Further significance concerning the weak influence of the liquid velocity on the lift-off process is discussed later.

The lift-off pdf's at various wall superheats are displayed in Fig. 3. It is seen that the mean lift-off diameter increases with increasing wall superheat.

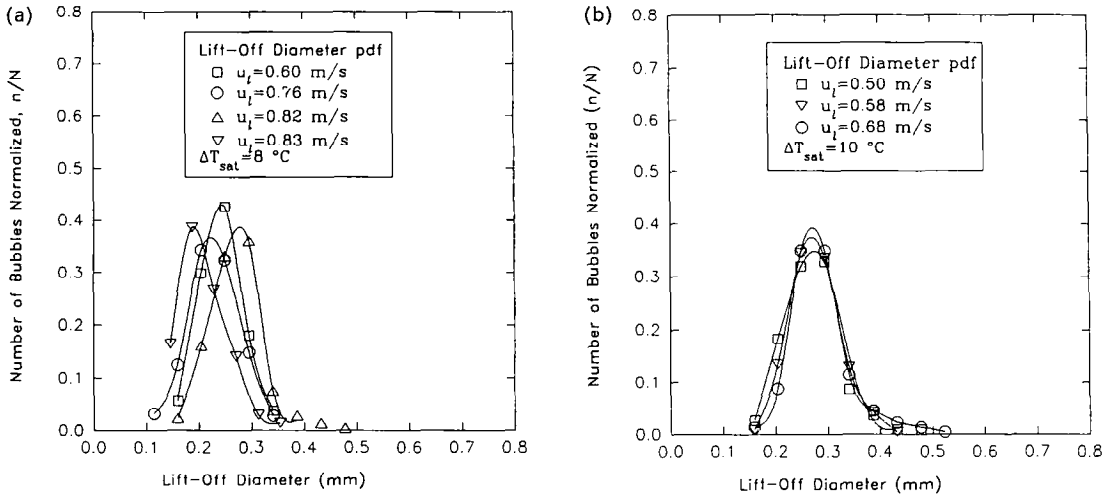

FIG. 2. Probability density functions of vapor bubble lift-off at various mean liquid velocities and constant wall superheat: (a) $\Delta T_{sat} = 8$ C, (b) $\Delta T_{sat} = 10$ C.

This trend is expected since the growth force, which retards vapor bubble lift-off, increases with increasing wall superheat. In the 12°C ΔT_{sat} case, the peak of the pdf is about the same as that for the 11°C case. It is expected that the peak for the 12°C ΔT_{sat} case should shift in the direction of increasing diameter. The fact that it does not is most likely attributable to some random scatter in the data as clearly observed in Fig. 2(a). A total of 37 lift-off data sets have been obtained. The mean lift-off diameters at various flow and thermal conditions are summarized in Table 1.

3. DEPARTURE AND LIFT-OFF MODEL

3.1. *Formulation*

The vapor bubble departure and lift-off model follows a similar form as that presented in ref. [4]. However, notable improvements have been adapted to the model which broaden its usefulness. Those improvements will be discussed in detail in the development which follows. Considering a vapor bubble attached to its nucleation site, as shown in Fig. 1, an x- and y-momentum equation for the bubble may be expressed as

$$\sum F_x = F_{sx} + F_{qs} + F_{dux} = \rho_v V_b \frac{du_{bcx}}{dt} \quad (1)$$

$$\sum F_y = F_{sy} + F_{duy} + F_{sL} + F_b + F_h + F_{cp} = \rho_v V_b \frac{du_{bcy}}{dt} \quad (2)$$

where F_s is the surface tension force, F_{qs} is the quasi-steady drag in the flow direction, F_{du} is the unsteady drag due to asymmetrical growth, F_{sL} is the shear lift force, F_b is the buoyancy force, F_h is the hydrodynamic pressure force, and F_{cp} is the contact pressure force which effectively includes the reaction of the wall to the vapor bubble, u_{bc} is the velocity of the bubble at its center of mass, V_b is the bubble volume, and ρ_v is the vapor density. A summary of the forces appearing in equations (1) and (2) have been enumerated in Table 2. The right hand side of (1) and (2) represents the acceleration of the vapor bubble in the respective x- and y-directions. For most cases of practical interest the acceleration is negligibly small while the bubble is attached to the heating surface because the dominant forces on the left hand sides of (1) and (2) are associated with $\rho_l (\gg \rho_v)$, and du_{bc}/dt is finite at the point of departure. It has been experimentally observed [4] that while a vapor bubble is attached to its nucleation site it is inclined in the flow direction at an angle θ_l due to the quasi-steady drag as depicted schematically in Fig. 1. It is postulated here that immediately following departure the bubble attempts to right itself such that the inclination angle approaches zero. Therefore, once the bubble departs its nucleation site it slides along the heating surface in the flow direction

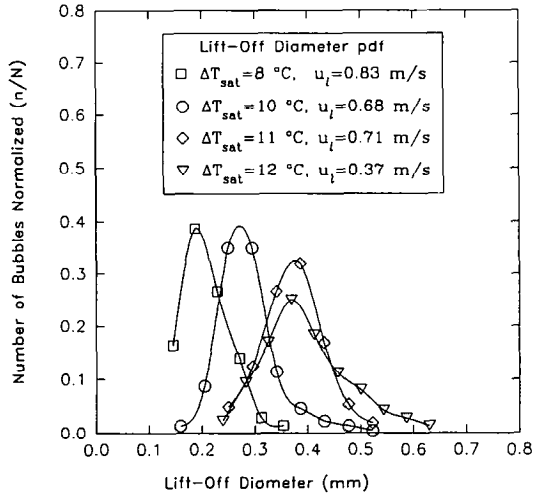

FIG. 3. Probability density functions of vapor bubble lift-off at various ΔT_{sat} and mean liquid velocity.

Table 1. Mean vapor bubble lift-off diameters

G (kg m^{-2} s^{-1})	X	T_{sat} (°C)	δ (mm)	$\bar{d}_L$ (mm)	q_w (kW^{-1} m^2)	ΔT_{sat} (°C)
237	0.167	63.0	4.1	0.20	8.2	5.2
203	0.045	60.6	6.7	0.24	5.8	5.5
237	0.169	63.1	4.2	0.19	10.0	5.9
255	0.077	61.5	5.7	0.29	8.1	6.0
254	0.107	61.8	4.7	0.27	8.5	6.5
273	0.088	61.8	5.3	0.26	9.1	6.8
203	0.046	60.6	6.6	0.27	7.6	7.2
222	0.106	61.0	4.9	0.30	9.1	7.6
199	0.039	60.6	6.2	0.28	7.8	7.8
191	0.127	60.8	4.8	0.24	9.4	8.1
276	0.157	61.2	3.1	0.19	8.5	8.1
237	0.169	62.8	4.1	0.21	13.5	8.2
150	0.043	60.1	6.6	0.36	6.6	8.2
273	0.084	61.8	5.7	0.23	12.2	8.3
155	0.100	59.5	6.8	0.30	7.3	8.3
255	0.080	61.4	5.7	0.28	10.7	8.4
255	0.102	61.7	4.8	0.27	11.8	8.4
222	0.067	60.4	5.5	0.31	10.3	8.7
222	0.106	60.9	4.7	0.35	11.1	9.1
262	0.114	61.1	4.5	0.24	13.1	9.1
162	0.107	60.7	5.1	0.36	8.8	9.1
255	0.103	61.8	4.9	0.26	14.2	9.3
200	0.041	60.4	6.5	0.28	10.8	9.5
250	0.083	61.5	5.8	0.28	12.8	9.5
251	0.117	60.1	4.0	0.32	13.2	9.6
203	0.051	60.5	6.7	0.27	11.5	9.8
251	0.080	61.4	5.8	0.29	14.3	9.8
315	0.159	61.9	3.9	0.21	12.1	9.9
192	0.121	60.6	5.0	0.28	12.8	10.0
222	0.071	60.0	5.6	0.32	13.1	10.2
251	0.114	60.1	4.0	0.33	15.8	10.5
273	0.085	61.9	5.5	0.26	16.8	10.6
150	0.045	60.0	6.4	0.46	8.7	11.0
226	0.065	59.5	6.0	0.34	15.6	11.0
162	0.109	60.7	5.0	0.40	12.6	11.2
200	0.048	59.2	6.2	0.29	14.3	11.5
149	0.045	59.8	6.7	0.40	11.9	11.6
154	0.123	59.5	6.1	0.31	7.9	12.0

($\bar{}$) Indicates an ensemble average.

with zero inclination angle until it lifts off the heating surface some finite distance downstream. This hypothesis is consistent with experimental observations.

Based on the above considerations, the *departure* point is reached when the condition that $\Sigma F_x = 0$ begins to be violated while $\Sigma F_y = 0$ is maintained. Once the vapor bubble rights itself such that $\theta_i = 0$, the bubble will slide along the heating surface until the condition $\Sigma F_y = 0$ is violated, at which point it will lift-off the heating surface. The two equations at the point of departure, $\Sigma F_x = 0$ and $\Sigma F_y = 0$, can be solved simultaneously for the departure diameter, d_d, and the inclination angle, θ_i. Therefore it is not necessary to specify θ_i to determine the departure diameter; θ_i results from the solution. This constitutes a major improvement over the departure model presented in ref. [4] in which θ_i was assumed constant and was determined empirically.

The forces listed in equations (1) and (2) were discussed in detail in ref. [4] and the manner in which they may be estimated was provided. Here it is recognized that certain forces dominate the departure and lift-off process and simplification of (1) and (2) may be achieved.

3.2. *Surface tension and contact pressure forces*

Expressions for the surface tension forces acting in the x- and y-direction were given in ref. [4]. Both F_{sx} and F_{sy} are directly proportional to the contact diameter, d_w. It was argued by Zeng *et al.* [5] that the contact diameter beneath a growing vapor bubble near the point of departure is sufficiently small such that the surface tension force is negligible compared with the buoyancy and growth forces. This argument was supported by the following: (1) due to the existence of a liquid microlayer beneath a growing vapor bubble the contact diameter should be small; (2) Cooper and Chandratilleke [6], Cooper *et al.* [7], and Zysin *et al.* [8] demonstrated that the contact diameter of a vapor bubble embedded in a superheated thermal layer is typically over estimated due to an index of refraction gradient which creates a mirage at the base of the bubble; and (3) a computational study by Lee

Table 2. Summary of forces appearing in momentum equations

Forces in momentum equation	Direction	Symbol	Expression given by	Force negligible	Reason for neglecting force
Surface tension	x	F_{sx}	Equation (6a) Ref. [4]	Yes	Supposition that $d_w \to 0$ at departure and lift-off
Quasi-steady drag	x	F_{qs}	Equation (3)	No	
Growth force	x	F_{dux}	Equations (8) and (9)	No	
Surface tension	y	F_{sy}	Equation (6b) Ref. [4]	Yes	Supposition that $d_w \to 0$ at departure and lift-off
Growth force	y	F_{duy}	Equations (8) and (9)	No	
Shear lift force	y	F_{sL}	Equation (5)	Only when considering lift-off	Bubble slides along surface with approximately same velocity as surrounding fluid
Buoyancy force	y	F_b	Equation (4)	No	
Hydrodynamic pressure force	y	F_h	Equation (6)	Yes	Supposition that $d_w \to 0$ at departure and lift-off, and $(d_w/a)^2 \ll 1$; $\therefore F_h \ll F_{sL}$ at a given ΔU
Contact pressure force	y	F_{cp}	Equation (24) Ref. [4]	Yes	Supposition that $d_w \to 0$ at point of departure and lift off, and $d_w/r_f \ll 1$; $\therefore F_{cp} \ll F_{sy}$

and Nydahl [9] indicates the surface tension force is an order of magnitude less than the buoyancy and growth forces near the departure point. The pool boiling departure model by Zeng *et al.* [5] was developed using the idea that the surface tension force is negligibly small near the departure point, and was found to give significantly improved predictions compared to empirical correlations which treated the surface tension as a dominant force. The same arguments are applicable to flow boiling, and thus F_{sx} and F_{sy} are assumed to be small in (1) and (2). As was mentioned earlier, direct proof of this assumption is currently lacking. Zeng *et al.* [5] also showed that the contact pressure force is generally smaller than the surface tension force and may be neglected.

3.3. *Quasi-steady drag, buoyancy, shear lift, and hydrodynamic pressure forces*

Using results from refs. [10] and [11], Klausner *et al.* [4] suggested that the quasi-steady drag, buoyancy, shear lift, and hydrodynamic pressure forces can be estimated from

$$\frac{F_{qs}}{6\pi\rho_l \nu \Delta U a} = \frac{2}{3} + \left[\left(\frac{12}{Re}\right)^n + 0.796^n\right]^{-1/n}, \qquad n = 0.65 \tag{3}$$

$$F_b = \frac{4}{3}\pi a^3(\rho_l - \rho_v)\, g \tag{4}$$

$$C_L = \frac{F_{sL}}{\frac{1}{2}\rho_l \Delta U^2 \pi a^2} = 3.877 G_s^{1/2}[Re^{-2} + 0.014 G_s^2]^{1/4} \tag{5}$$

$$G_s = \left|\frac{dU}{dy}\right| \frac{a}{\Delta U}$$

$$F_h = \frac{9}{8}\rho_l \Delta U^2 \frac{\pi d_w^2}{4} \tag{6}$$

where ΔU is the relative velocity between the bubble center of mass and liquid, a the bubble radius, $Re = 2\Delta U a/\nu$ the bubble Reynolds number, g the gravitational acceleration, and ν the liquid kinematic viscosity. The liquid velocity profile near the wall is estimated using Reichardt's single-phase turbulent flow expression

$$\frac{U(y)}{u^*} = \frac{1}{\kappa}\ln\left(1 + \kappa\frac{yu^*}{\nu}\right) + c\left[1 - \exp\left(-\frac{yu^*/\nu}{\chi}\right) - \frac{yu^*/\nu}{\chi}\exp\left(-0.33\frac{yu^*}{\nu}\right)\right] \tag{7}$$

where $\kappa = 0.4$, $\chi = 11$, and $c = 7.4$. Noting that the bulk turbulence for two-phase flow is more intense than that for single-phase flow, $u^*/u_l = 0.05$ has been assumed, where $u_l = G(1-X)D/\rho_l\delta$ is the mean liquid velocity of the two-phase mixture, δ the liquid film thickness, and D the inner dimension of the square channel.

Since the shear lift coefficient is an order 1 quantity and $(d_w/a)^2 \ll 1$ near the lift-off point, the hydrodynamic pressure force is typically negligible compared with the shear lift force for a given ΔU. In order to evaluate F_{sL}, information on ΔU is required. However, once the vapor bubble departs its nucleation site, it begins sliding along the heating surface and thus the relative velocity, ΔU, is difficult to

estimate. In order to resolve this dilemma consideration is given to the lift-off diameter experiments reported above. It was demonstrated in Figs. 2(a) and (b) that the mean lift-off diameter shows virtually no dependence on the mean liquid velocity. The most plausible explanation for this observation is that the bubble slides along the heating surface with approximately the same velocity as the surrounding liquid, in which case ΔU, and hence the shear lift force, are small. High speed cinematography, using a Hycam camera operating at 5000 frames per second, was used to measure the sliding velocity of departed vapor bubbles. The estimated measuring error is ± 0.01 m s^{-1}. For boiling conditions of $u_l = 0.47$ m s^{-1}, $\Delta T_{sat} = 9.3$ C, and $T_{sat} = 71.6$ C the average measured sliding velocity based on an observation of 4 bubbles is 0.14 m s^{-1}. The average liquid velocity at the bubble center of mass, calculated from equation (7), is also 0.14 m s^{-1}. The fact that the velocities are identical is coincidental because an observation of 4 bubbles is not sufficient to obtain a statistically reliable average. Nevertheless, this measurement indicates that the average velocity of the bubble and that of the liquid are at least close, and it provides valuable evidence supporting the above hypothesis. Under such circumstances both the shear lift force and hydrodynamic pressure force will be small compared with the buoyancy force and are thus neglected for the case of sliding bubbles in horizontal flow boiling under one-g conditions.

3.4. *Growth force*

Klausner *et al.* [4] modelled the growth force by considering a hemispherical bubble expanding in an inviscid liquid. Zeng *et al.* [5] modified the expression with the introduction of an empirical constant, C_s, which was believed to account for the presence of a wall. The growth force expression given by Zeng *et al.* [5] is used here,

$$F_{du} = -\rho_l \pi a^2 \left(\frac{3}{2} C_s \dot{a}^2 + a\ddot{a} \right) \tag{8}$$

where ($\dot{}$) indicates differentiation with respect to time. For pool boiling it was found that $C_s = 20/3$ provides the best fit to the data, and the same value is used for flow boiling. When the bubble is inclined in the flow direction with an angle, θ_i, the force due to unsteady growth in the respective x- and y-directions may be estimated from

$$F_{dux} = F_{du} \sin \theta_i \quad \text{and} \quad F_{duy} = F_{du} \cos \theta_i. \tag{9}$$

In order to estimate accurately the growth force, information on the bubble growth rate is required. A bubble growth rate expression for a bubble growing in a nonuniform temperature field which adequately accounts for variations in pressure, gravitational field, and bubble shape does not currently exist. In ref. [5] it was suggested that Zuber's [12] diffusion controlled bubble growth solution is useful for pool boiling under one-g subatmospheric and atmospheric pressure conditions

$$a(t) = \frac{2b}{\sqrt{\pi}} Ja \sqrt{(\eta t)} \tag{10}$$

where

$$Ja = \frac{\rho_l C_{pl} \Delta T_{sat}}{\rho_v h_{fg}}$$

and Ja is the Jakob number, η the liquid thermal diffusivity, C_{pl} the liquid specific heat, h_{fg} the latent heat of vaporization, and b an empirical constant which is supposed to account for asphericity. Zuber's bubble growth model is used here because it agrees reasonably well with limited available flow boiling vapor bubble growth data, it is simple, and it allows for b to be adjusted to fit experimental observations.

Sample measurements of vapor bubble growth rate of refrigerant R113 using the current experimental facility were obtained via high speed cinematography. A Fastax camera was utilized which was operated at up to 6000 frames per second. The maximum resolution of the measurements is 0.004 mm. The vapor bubble growth rate is displayed in Fig. 4 for five different bubbles from the same nucleation site for the following conditions: mean wall superheat, $\Delta T_{sat} = 8.2$°C and mass flux, $G = 155$ kg m^{-2} s^{-1}. It was found that $b = 1.73$ provides the best fit to the data. Other measurements have been obtained in which b ranges from 1 to 1.73 depending on the flow conditions and location of the nucleation site. It is emphasized that $\Delta T_{sat} = 8.2$°C in Fig. 4 is the measured mean wall superheat and is not like the local wall superheat seen by the nucleation site. Since the wall temperature field is nonuniform, the bubble growth rate for an individual bubble will depend on the local wall superheat as opposed to the mean. Nevertheless, it has been found that when (10) is used

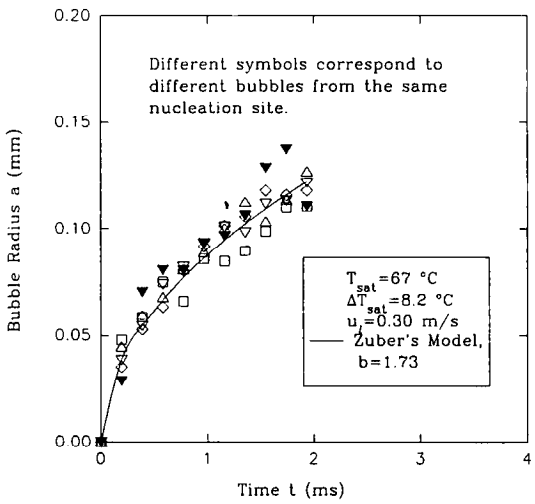

FIG. 4. Vapor bubble growth rate at $\Delta T_{sat} = 8.2$°C and $T_{sat} = 67$°C.

with (8), best results for predicting the mean departure and lift-off diameters are obtained with $b = 1.0$.

3.5. *Final equations used for calculating vapor bubble departure and lift-off diameters*

Based on the above approximations, the following equations result in an estimate for the mean departure diameter and inclination angle when the bubble departs the nucleation site via sliding,

$$F_{qs}+F_{du}\sin\theta_i = 0 \quad \text{and} \quad F_b+F_{du}\cos\theta_i+F_{sL} = 0. \tag{11}$$

The corresponding estimate for the lift-off diameter may be calculated from

$$F_b+F_{du} = 0; \qquad \theta_i = 0. \tag{12}$$

It is seen that the criteria for vapor bubble lift-off in flow boiling is identical to the departure criteria for pool boiling reported by Zeng *et al.* [5]. However, flow boiling lift-off diameters will be typically smaller than the departure diameters for pool boiling since the wall superheat, which controls the vapor bubble growth rate, is smaller for flow boiling due to the additional energy transport from the wall to the bulk liquid provided by bulk turbulent convection.

4. COMPARISON OF DEPARTURE AND LIFT-OFF MODEL WITH EXPERIMENTAL DATA

From the foregoing analysis, it is seen that when the wall superheat is fixed, the vapor bubble departure diameter is a function of only the mean liquid velocity. Measurements of mean departure diameter over a range of u_l and ΔT_{sat} were presented in ref. [4] and are used here for comparison. Figure 5 shows the measured departure diameters as a function of mean liquid velocity in which the wall superheat was maintained in a range of 14–16°C. Also shown are the predicted departure diameters using the current departure model for $\Delta T_{sat} = 15$°C and the model presented in ref. [4] for $\Delta T_{sat} = 15$°C and $d_w = 0$. It is seen that very good agreement exists with the current model. A comparison between the measured and predicted departure diameters, obtained under different flow and thermal conditions, for all of the data is shown in Fig. 6. The relative deviation, *r.d.*, was defined in ref. [4] as

$$r.d. = \frac{\sum_{k=1}^{N} \frac{|d_{meas,k}-d_{pred,k}|}{d_{meas,k}}}{N} \times 100 \tag{13}$$

where N is the number of data points, and the subscripts 'meas' and 'pred' refer to the respective measured and predicted diameters. The relative deviation is useful for characterizing the performance of the departure and lift-off model. For the data shown in Fig. 6, *r.d.* = 18% which is acceptable considering the departure diameter is sensitive to the vapor bubble growth rate which was calculated using equation (10). It seems that when the present model is compared to that reported in ref. [4] in which d_w was assumed finite and θ_i assumed constant, no improvement is gained in the prediction of the departure diameter. However, it should be recognized that the present model is substantially more useful since empirical data concerning θ_i and d_w are not required. In addition, the performance of the departure model is improved when the vapor bubble growth rate is known, and evidence is provided by considering the departure of individual bubbles displayed in Table 3, which were obtained using high speed cinematography. In general, the vapor bubble growth rate may be expressed as a power law

$$a(t) = Kt^n \tag{14}$$

where K and n must be determined from bubble growth rate measurements. The values of K and n for each bubble in Table 3 are also reported. The pre-

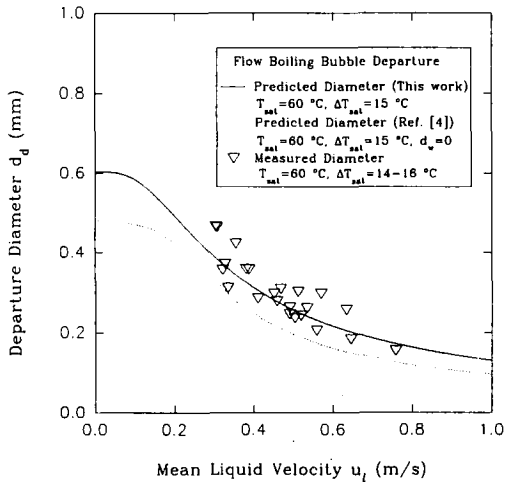

FIG. 5. Departure diameter variation with mean liquid velocity at approximately same ΔT_{sat}.

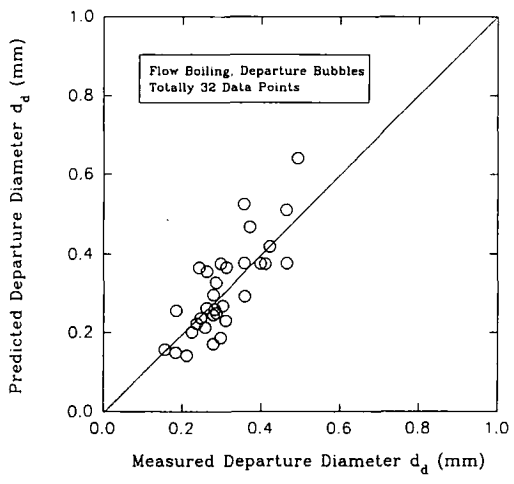

FIG. 6. Comparison between predicted and measured departure diameters.

Table 3. Measured and predicted departure diameters based on high speed cinematography data

$d_{d,meas}$ (mm)	$d_{d,pred}$ (mm)	Relative error (%)	K† ($\times 10^3$)	n	u_l ($m^{-1}s^{-1}$)	ΔT_{sat} (°C)	T_{sat} (°C)
0.256	0.259	1.2	1.94	0.435			
0.240	0.220	8.4	1.29	0.382			
0.221	0.218	1.3	1.84	0.450	0.30	8.2	67.0
0.245	0.243	0.8	1.79	0.429			
0.240	0.220	8.4	1.16	0.362			
0.121	0.115	4.6	0.97	0.428			
0.123	0.115	6.8	0.57	0.334			
0.142	0.138	2.8	1.07	0.421	0.28	10.0	71.0
0.150	0.153	2.2	1.10	0.410			
0.138	0.148	6.9	0.94	0.386			

† Indicates units on K are such that when applied to equation (14) the radius dimension is meters.

dicted departure diameters displayed in Table 3 were calculated using (14) in lieu of (10). It is seen that the prediction is significantly improved, and the relative deviation for the predicted departure diameters in Table 3 is 4%.

Figure 7 shows the predicted mean departure diameter using the present model as a function of liquid velocity and wall superheat. The observed trend, departure diameter decreases with increasing liquid velocity and increases with increasing wall superheat, was reported by Klausner *et al.* [4]. Figure 8 shows the predicted inclination angle as a function of the predicted departure diameter. It is seen that the predicted inclination angle varies from about 5 to 25 degrees. Although an accurate measurement of the inclination angle with the present experimental facility is not currently achievable, the predicted inclination angle falls in a range which is consistent with experimental observations. In addition, Fig. 8 shows that the departure diameter decreases with increasing inclination angle. This trend is expected since the inclination angle should increase with increasing u_l, and the trend in Fig. 5 shows departure diameter decreases

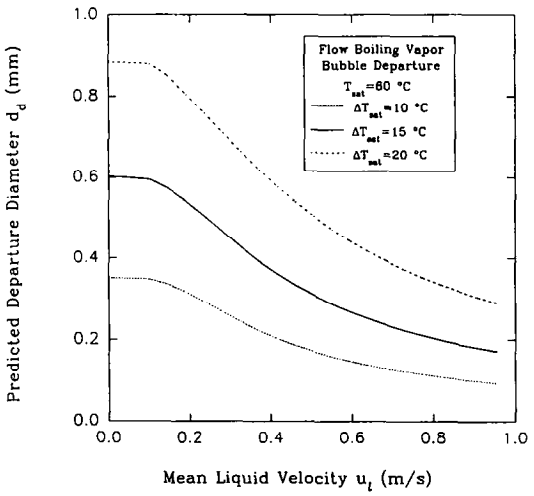

FIG. 7. Departure diameter variation with mean liquid velocity and ΔT_{sat}.

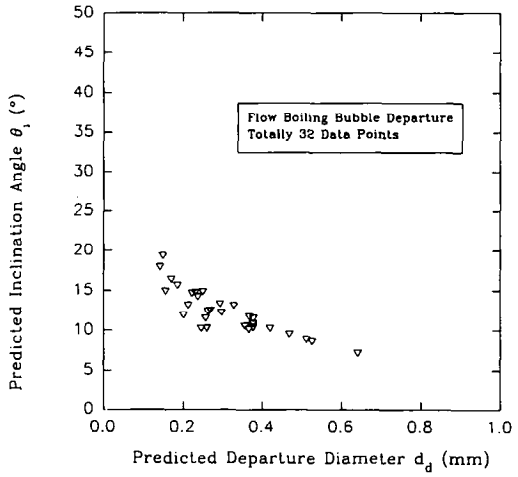

FIG. 8. Predicted inclination angle variation with predicted departure diameter.

with increasing u_l. In Figure 9 the predicted inclination angle is shown as a function of liquid velocity at various wall superheats. While θ_i increases with increasing velocity, it decreases with increasing wall superheat.

Figure 10 shows the predicted lift-off diameters against the measured values. The relative deviation for the data in Fig. 10 is 19% which is acceptable. The relative deviations measured for the departure and lift-off diameters are comparable to those reported by Zeng *et al.* [5] for their pool boiling model.

In the limiting case of zero liquid velocity, the criterion for bubble departure is identical to that of the pool boiling model suggested by Zeng *et al.* [5]. Although only a limited number of flow boiling departure and lift-off data are currently available for comparison against the above model, it is encouraging that when tested in the pool boiling limit, the above model agrees very well with data obtained over a wide range of conditions [5].

5. DISCUSSION

A general model has been presented which adequately predicts vapor bubble departure and lift-

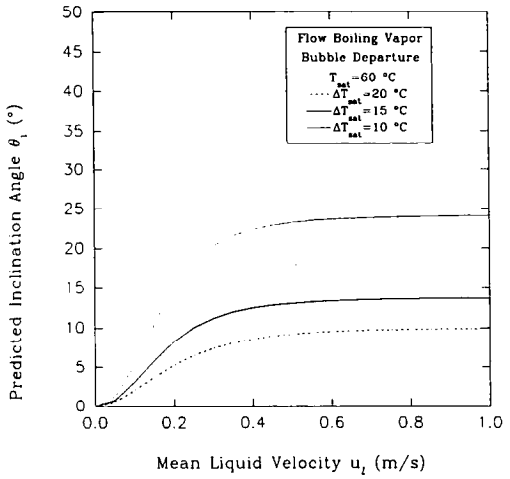

FIG. 9. Predicted inclination angle variation with mean liquid velocity and ΔT_{sat}.

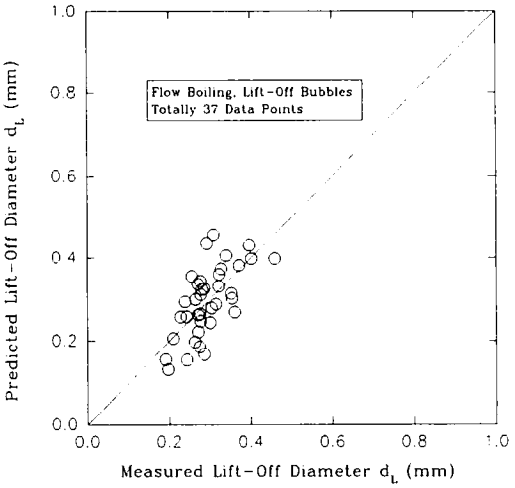

FIG. 10. Comparison between predicted and measured lift-off diameters.

off diameters for horizontal flow boiling. The only required input is the vapor bubble growth rate, which may be approximated from equation (10) for low pressure systems. In theory, the model is also applicable to vertical flow boiling although calibration of the model is required. For example, it was assumed that $u^*/u_l = 0.05$ for horizontal two-phase flow when evaluating the liquid velocity profile given by equation (7). If equation (7) is even applicable to vertical flow it is expected that $u^*/u_l > 0.05$ due to enhanced bulk turbulence.

For the vertical downflow boiling configuration, a sliding bubble should lag the liquid velocity due to the buoyancy force. Thus a shear lift force will exist which pushes the bubble away from the wall. Thus bubble removal from the wall may be accomplished via the shear lift force. For vertical upflow boiling, the sliding bubble velocity should lead that of the liquid, and thus the resulting shear lift force will push the bubble against the wall. Thus bubble removal from the wall will be hampered by the shear lift force. However, the bubble continues to grow while it slides which may result in a strong unsteady, large scale, 3-dimensional two-phase flow. The bubble could either be removed by large transverse velocity fluctuations or continue to grow until it merges with the bulk two-phase mixture. The present model is not applicable under such circumstances. Under microgravity flow boiling conditions the sliding bubble velocity should closely follow that of the liquid, and both the shear lift and buoyancy forces will be absent. The bubble will continue to grow until strong 3-dimensional disturbances are created in the bulk liquid flow. The bubble will possibly be removed by transverse liquid velocity fluctuations or simply merge into the bulk two-phase mixture. Again, the present model is not applicable under such circumstances.

Acknowledgement—This material is based on work supported by the National Science Foundation under Grant No. CTS-9008269. The undergraduate research assistance provided by J. N. Brouillette in obtaining high-speed motion-pictures of vapor bubble growth is greatly appreciated.

REFERENCES

1. Y. P. Chang, Some possible critical conditions in nucleate boiling, *J. Heat Transfer* **85**(2), 89–100 (1963).
2. S. Levy, Forced convection subcooled boiling-prediction of vapor volumetric fraction, *Int. J. Heat Mass Transfer* **10**, 951–965 (1967).
3. N. Koumoutsos, R. Moissis and A. Spyridonos, A study of bubble departure in forced-convection boiling, *J. Heat Transfer* **90**, 223–230 (1968).
4. J. F. Klausner, R. Mei, D. M. Bernhard and L. Z. Zeng, Vapor bubble departure in forced convection boiling, *Int. J. Heat Mass Transfer* **36**, 651–662 (1993).
5. L. Z. Zeng, J. F. Klausner and R. Mei, A unified model for the prediction of bubble detachment diameters in boiling systems—I. Pool boiling, *Int. J. Heat Mass Transfer* **36**, 2261–2270 (1992).
6. M. G. Cooper and T. T. Chandratilleke, Growth of diffusion-controlled vapor bubbles at a wall in a known temperature gradient, *Int. J. Heat Mass Transfer* **24**, 1475–1492 (1981).
7. M. G. Cooper, K. Mori and C. R. Stone, Behavior of vapor bubbles growing at a wall with forced flow, *Int. J. Heat Mass Transfer* **26**, 1489–1507 (1983).
8. L. V. Zysin, L. A. Fel'Dberg, A. L. Dobkes and A. G. Sazhenin, Allowance for optical distortion produced by temperature gradients in investigating the shape of vapor bubbles generated on a flat wall, *Heat Transfer—Sov. Res.* **12**, 6–10 (1980).
9. R. C. Lee and J. E. Nydahl, Numerical calculation of bubble growth in nucleate boiling from inception through departure, *J. Heat Transfer* **111**, 474–479 (1989).
10. R. Mei and J. F. Klausner, Unsteady force on a spherical bubble at finite Reynolds number with small fluctuations in the free-stream velocity, *Physics of Fluids* A, **4**(1), 63–70 (1992).
11. R. Mei and J. F. Klausner, Shear lift force on spherical bubbles, submitted to *Int. J. Heat and Fluid Flow* (1992).
12. N. Zuber, The dynamics of vapor bubbles in nonuniform temperature fields, *Int. J. Heat Mass Transfer* **2**, 83–98 (1961).